Conceptual designs of a laser plasma accelerator-based EUV-FEL and an all-optical Gamma-beam source

Kazuhisa Nakajima

Center for Relativistic Laser Science, Institute for Basic Science (IBS), Gwangju 500-712, Republic of Korea

Abstract
Recently, intense research into laser plasma accelerators has achieved great progress in the production of high-energy, high-quality electron beams with GeV-level energies in a cm-scale plasma. These electron beams open the door for broad applications in fundamental, medical, and industrial sciences. Here we present conceptual designs of an extreme ultraviolet radiation source for next-generation lithography and a laser Compton Gamma-beam source for nuclear physics research on a table-top scale.

Keywords: high peak high average power lasers; laser wakefield accelerators

1. Introduction

To date, intense research has been carried out on laser plasma acceleration concepts[1] to achieve high-energy, high-quality electron beams with GeV energies in a cm-scale plasma[2–6], a 1%-level energy spread[7], a 1 mm mrad level transverse emittance[8], and a 1 fs level bunch duration[9], ensuring that the stability of reproduction is as high as that of present high-power ultra-short-pulse lasers[10]. Recently, staged laser plasma acceleration[11–13] has been successfully demonstrated in conjunction with ionization-induced injection[14–16] and phase-locking acceleration[17]. Relativistic electron beams from ultraintense laser plasma interactions can be conceived to be compact particle accelerators, inspiring a wide range of applications of unique particle beam and radiation sources, such as THz[18, 19] and X-ray/Gamma-ray radiation[20–25].

Here we present an extreme ultraviolet (EUV) radiation source for next-generation lithography and a laser Compton Gamma-beam source for nuclear physics research. EUV lithography with wavelengths below 13.5 nm is capable of providing resolution below 30 nm in semiconductor manufacturing. We propose a self-amplified spontaneous emission (SASE) free electron laser (FEL) driven by relativistic electron beams from laser plasma accelerators. For example, this FEL system, capable of generating an average EUV power of 1 kW at 13.5 nm, comprises a fiber-based chirped pulse amplification (CPA) laser delivering a 1 MW average laser power, a 5 cm gas cell-type plasma accelerator producing a 660 MeV electron beam with a 1.6% relative energy spread and a 0.5 nC charge, and a 1 m long undulator with a 15 mm period and a 1.4 T peak magnetic field.

High-quality Gamma beams generated from inverse Compton scattering off relativistic electron beams interacting with an intense laser pulse have aroused interest in photonuclear physics and nuclear astrophysics research, the characterization of nuclear materials or radioactive waste and so on. We present a table-top all-optical laser plasma accelerator-based Gamma-beam source comprising a high-power laser system with synchronous dual outputs, a laser plasma accelerator producing 300–900 MeV electron beams, and scatter optics whereby the laser pulse is focused onto the electron beam to generate a Gamma beam via Compton scattering with photon energies of 2–20 MeV.

2. Design of laser plasma accelerators for driving electron beams

2.1. Accelerator stage

Most of the laser plasma acceleration experiments that have successfully demonstrated the production of quasi-monoenergetic electron beams with a narrow energy spread have been elucidated in terms of self-injection and acceleration mechanisms in the bubble regime[26, 27], where a drive laser pulse with wavelength λ_L, peak power P_L, intensity I_L, and focused spot radius r_L is characterized by a normalized vector potential $a_0 \gg 1$ with respect to the electron rest energy mc^2, given for the linear polarization as

Correspondence to: K. Nakajima, Center for Relativistic Laser Science, Institute for Basic Science (IBS), Gwangju 500-712, Republic of Korea. Email: naka115@dia-net.ne.jp

$$a_0 = \left(\frac{2e^2 \lambda_L^2 I_L}{\pi m^2 c^5} \right)^{1/2}$$

$$\cong 8.55 \times 10^{-10} \sqrt{I_L(\mathrm{W\,cm^{-2}})} \lambda_L \ (\mu\mathrm{m})$$

$$\approx 6.82 \sqrt{P_L(\mathrm{TW})} \frac{\lambda_L}{r_L}. \tag{1}$$

In these experiments, electrons are self-injected into a non-linear wake, often referred to as a bubble, i.e., a cavity void of plasma electrons consisting of a spherical ion column surrounded by a narrow electron sheath, formed behind the laser pulse instead of a periodic plasma wave in the linear regime. The phenomenological theory of nonlinear wakefields in the bubble (blowout) regime[26] describes the accelerating wakefield $E_z(\xi)/E_0 \approx (1/2)k_p\xi$ in the bubble frame moving in a plasma with velocity v_B, i.e., $\xi = z - v_B t$, where $k_p = \omega_p/c = (4\pi r_e n_e)^{1/2}$ is the plasma wavenumber evaluated with a plasma frequency ω_p, an unperturbed on-axis electron density n_e and the classical electron radius $r_e = e^2/mc^2$, and $E_0 = mc\omega_p/e$ is the non-relativistic wave-breaking field, approximately given by $E_0 \approx 96 \ (\mathrm{GV\,m^{-1}})(n_e/10^{18} \ (\mathrm{cm^{-3}}))^{1/2}$. In the bubble regime for $a_0 \geqslant 2$, since an electron-evacuated cavity shape is determined by balancing the Lorentz force of the ion sphere exerted on the electron sheath with the ponderomotive force of the laser pulse, the bubble radius R_B is approximately given as $k_p R_B \approx 2\sqrt{a_0}$[27]. Thus, the maximum accelerating field is given by $E_{z0}/E_0 = (1/2)\alpha k_p R_B$, where α represents a factor taking into account the difference between the theoretical estimation and the accelerating field reduction due to the beam loading effects.

Here we consider the self-guided case, where a drive laser pulse propagates in a homogeneous density plasma. The equations of longitudinal motion of an electron with normalized energy $\gamma = E_b/mc^2$ and longitudinal velocity $\beta_z = v_z/c$ are written approximately as[28]

$$\frac{d\gamma}{dz} = \frac{1}{2}\alpha k_p^2 R_B \left(1 - \frac{\xi}{R_B} \right),$$

$$\frac{d\xi}{dz} = 1 - \frac{\beta_B}{\beta_z} \approx 1 - \beta_B \approx \frac{3}{2\gamma_g^2}, \tag{2}$$

where $\xi = z - v_B t$ $(0 \leqslant \xi \leqslant R_B)$ is the longitudinal coordinate of the bubble frame moving at a velocity of $v_B = c\beta_B \approx v_g - v_{\mathrm{etch}}$, taking into account diffraction at the laser pulse front that etches back at a velocity $v_{\mathrm{etch}} \sim ck_p^2/k^2$[27] with laser wavenumber k, and $\gamma_g = (1 - \beta_g^2)^{-1/2} \approx k/k_p \gg 1$ is assumed. Integrating Equations (2), the energy and phase of the electron can be calculated as[28]

$$\gamma(z) = \gamma_0 + \frac{1}{3}\alpha\gamma_g^2 k_p^2 R_B \xi(z)\left(1 - \frac{1}{2}\frac{\xi(z)}{R_B} \right),$$

$$\xi(z) = \frac{3}{2}\frac{z}{\gamma_g^2}, \tag{3}$$

where $\gamma_0 = \gamma(0)$ is the injection energy. Hence, the maximum energy gain is obtained at $\xi = R_B$ as

$$\Delta\gamma_{\mathrm{max}} = \gamma_{\mathrm{max}} - \gamma_0 \approx \frac{1}{6}\alpha\gamma_g^2 k_p^2 R_B^2 \approx \frac{2}{3}\alpha a_0 \gamma_g^2$$

$$= \frac{2}{3}\alpha\kappa_{\mathrm{self}} a_0 \frac{n_c}{n_e}, \tag{4}$$

where κ_{self} is the correction factor of the relativistic factor for the group velocity in a uniform plasma for a self-guided pulse, i.e., $\gamma_g^2 = (1 - \beta_g^2)^{-1} \approx \kappa_{\mathrm{self}} k^2/k_p^2 = \kappa_{\mathrm{self}} n_c/n_e$, obtained from[28]

$$\kappa_{\mathrm{self}} = \frac{a_0^2}{8}\left(\sqrt{1 + a_0^2/2} - 1 - \ln\frac{\sqrt{1 + a_0^2/2} + 1}{2} \right)^{-1}, \tag{5}$$

and $n_c = m\omega_L^2/4\pi e^2 = \pi/(r_e\lambda_L^2) \approx 1.115 \times 10^{21} \ (\mathrm{cm^{-3}})$ $(\lambda_L/1 \ \mu\mathrm{m})^{-2}$ is the critical plasma density. The dephasing length L_{dp} for the self-guided bubble regime is given by

$$k_p L_{\mathrm{dp}} \approx \frac{2}{3}k_p R_B \gamma_g^2 = \frac{4}{3}\sqrt{a_0}\kappa_{\mathrm{self}}\frac{n_c}{n_e}. \tag{6}$$

For a given energy gain E_b, the operating plasma density is determined from Equation (4) as

$$n_e = \frac{2}{3}\alpha\kappa_{\mathrm{self}} a_0 \frac{n_c}{\Delta\gamma_{\mathrm{max}}}$$

$$\approx 1.9 \times 10^{18} \ (\mathrm{cm^{-3}})\kappa_{\mathrm{self}} a_0$$

$$\times \left(\frac{1 \ \mu\mathrm{m}}{\lambda_L} \right)^2 \left(\frac{200 \ \mathrm{MeV}}{E_b/\alpha} \right). \tag{7}$$

The accelerator length equal to the dephasing length becomes

$$L_{\mathrm{acc}} = L_{\mathrm{dp}} \approx \sqrt{\frac{3}{2}}\frac{(\Delta\gamma_{\mathrm{max}}/\alpha)^{3/2}}{\pi\kappa_{\mathrm{self}}^{1/2} a_0}\lambda_L$$

$$\approx \frac{3.1 \ (\mathrm{mm})}{\kappa_{\mathrm{self}}^{1/2} a_0}\left(\frac{\lambda_L}{1 \ \mu\mathrm{m}} \right)\left(\frac{E_b/\alpha}{200 \ \mathrm{MeV}} \right)^{3/2}, \tag{8}$$

while the pump depletion length due to pulse-front erosion is given by

$$L_{\mathrm{pd}} \approx c\tau_L \frac{n_c}{n_e} = \frac{3}{2}\frac{c\tau_L \Delta\gamma_{\mathrm{max}}/\alpha}{\kappa_{\mathrm{self}} a_0}$$

$$\approx \frac{5 \ (\mathrm{mm})}{\kappa_{\mathrm{self}} a_0}\left(\frac{\tau_L}{30 \ \mathrm{fs}} \right)\left(\frac{E_b/\alpha}{200 \ \mathrm{MeV}} \right). \tag{9}$$

The dephasing length should be less than the pump depletion length, i.e., $L_{\mathrm{pd}} \geqslant L_{\mathrm{dp}}$. Thus, the required pulse duration for self-guiding of the drive laser pulse is given by

$$\tau_L \geqslant 18 \text{ (fs)} \kappa_{\text{self}}^{1/2} \left(\frac{\lambda_L}{1\,\mu\text{m}} \right) \left(\frac{E_b/\alpha}{200\,\text{MeV}} \right)^{1/2}. \quad (10)$$

The matched spot radius becomes

$$r_m \approx 3.9 \text{ (\mu m)} \frac{R_m}{\sqrt{\kappa_{\text{self}}}a_0} \left(\frac{\lambda_L}{1\,\mu\text{m}} \right) \left(\frac{E_b/\alpha}{200\,\text{MeV}} \right)^{1/2}, \quad (11)$$

where $R_m \equiv k_p r_L$ is the dimensionless matched spot radius given by[28]

$$R_m = \left\{ \frac{\ln(1+a_0^2/2)}{\sqrt{1+a_0^2/2} - 1 - 2\ln[(\sqrt{1+a_0^2/2}+1)/2]} \right\}^{1/2}. \quad (12)$$

The corresponding matched power is calculated as

$$P_L = \frac{k_p^2 r_L^2 a_0^2}{32} P_c \approx 0.312 \text{ (TW)} \frac{a_0 R_m^2}{\kappa_{\text{self}}} \left(\frac{E_b/\alpha}{200\,\text{MeV}} \right). \quad (13)$$

The required pulse energy becomes

$$U_L = P_L \tau_L \geqslant 5.62 \text{ (mJ)} \frac{a_0 R_m^2}{\kappa_{\text{self}}^{1/2}} \left(\frac{\lambda_L}{1\,\mu\text{m}} \right) \left(\frac{E_b/\alpha}{200\,\text{MeV}} \right)^{3/2}. \quad (14)$$

2.2. Beam loading effects

In laser wakefield acceleration, an accelerated electron beam induces its own wakefield and cancels the laser-driven wakefield. Assuming the beam loading efficiency $\eta_b \equiv 1 - E_z^2/E_M^2$ defined by the fraction of plasma wave energy absorbed by particles of the bunch with a root mean square (r.m.s.) radius σ_b, the beam-loaded field is given by $E_z = \sqrt{1-\eta_b}E_M = \alpha E_M$, where E_M is the accelerating field without beam loading, given by $E_M \approx a_0^{1/2} E_0$ for the bubble regime $a_0 \geqslant 2$. Thus, a loaded charge is calculated as[29]

$$Q_b \simeq \frac{e}{4k_L r_e} \frac{\eta_b k_p^2 \sigma_b^2}{1-\eta_b} \frac{E_z}{E_0} \left(\frac{n_c}{n_e} \right)^{1/2}$$

$$\approx 76 \text{ (pC)} \frac{\eta_b a_0^{1/2} k_p^2 \sigma_b^2}{\sqrt{1-\eta_b}} \left(\frac{n_e}{10^{18}\,\text{cm}^{-3}} \right)^{-1/2}. \quad (15)$$

Using the plasma density Equation (7), the loaded charge is given by

$$Q_b \approx 55 \text{ (pC)} \frac{1-\alpha^2}{\alpha^{3/2}} \frac{k_p^2 \sigma_b^2}{\kappa_{\text{self}}^{1/2}} \left(\frac{\lambda_L}{1\,\mu\text{m}} \right) \left(\frac{E_b}{200\,\text{MeV}} \right)^{1/2}. \quad (16)$$

Therefore, the field reduction factor α for accelerating charge Q_b up to energy E_b is obtained by solving the equation

$$\alpha^2 + C\alpha^{3/2} - 1 = 0, \quad (17)$$

where the coefficient C is defined as

$$C \equiv \frac{Q_b}{55 \text{ (pC)}} \frac{\kappa_{\text{self}}^{1/2}}{k_p^2 \sigma_b^2} \left(\frac{1\,\mu\text{m}}{\lambda_L} \right) \left(\frac{200\,\text{MeV}}{E_b} \right)^{1/2}. \quad (18)$$

2.3. Injector stage

Electron beams can be produced and accelerated in the injector stage driven by the same laser pulse as that in the accelerator stage, relying on a self-injection mechanism such as the expanding bubble self-injection mechanism[30] or an ionization-induced injection scheme with a short mixed gas cell[14–16, 31], where tunnel ionization leads to electron trapping near the centre of the laser wakefield. Here we consider the ionization-induced injection scheme. According to theoretical considerations in ionization-induced injection[31], for trapping electrons ionized at the peak of the laser electric field, the minimum laser intensity is given by $1 - \gamma_g^{-1} \leqslant 0.64a_{\min}^2$. At a plasma density $n_{\text{inj}} = 10^{18}$ cm^{-3} in the injector, the required minimum laser field is $a_{\min} \geqslant 1.23$. The maximum number of trapped electrons saturates at approximately $N_{e\,\text{max}} \sim 5 \times 10^6$ μm^{-2} at a gas length $L_{\text{inj}} \approx 1000\lambda_L$ for a plasma density $n_{\text{inj}} = 0.001 n_c$ with a nitrogen concentration of $\alpha_N = 1\%$ and laser parameters of $a_0 = 2$ and $c\tau_L \approx 15\lambda_L$ due to the beam loading effects and initially trapped particle loss from the separatrix in the phase space. From the particle-in-cell (PIC)-simulation results[31], the trapped electron density scales as

$$N_e \text{ (\mu m}^{-2}) \sim 8 \times 10^7 \alpha_N k_p L_{\text{inj}} \left(\frac{n_{\text{inj}}}{n_c} \right)^{1/2}$$

$$\approx 5 \times 10^8 \alpha_N \left(\frac{L_{\text{inj}}}{\lambda_L} \right) \left(\frac{n_{\text{inj}}}{n_c} \right). \quad (19)$$

The energy spread is also proportional to both the mixed gas length and the nitrogen concentration. In a injector with gas length L_{inj}, the electron charge Q_b trapped inside a bunch with radius $r_b = 1/k_p \approx 5.3$ $(\mu$m$)$ at $n_{\text{inj}} = 10^{18}$ cm^{-3} is estimated as

$$Q_b \sim \frac{k_p^2 r_b^2}{4r_e n_{\text{inj}}} e N_e \approx 6.4 \text{ (pC)} \alpha_N k_p^2 r_b^2 \left(\frac{\lambda_L}{1\,\mu\text{m}} \right) \left(\frac{L_{\text{inj}}}{1\,\mu\text{m}} \right). \quad (20)$$

An electron charge of 500 pC will be trapped via the ionization-induced injection mechanism in an injector gas cell with a 2 mm length and a nitrogen concentration of $\alpha_N = 4\%$.

2.4. Design of a SASE FEL

In the SASE FEL process, coupling the electron bunch with a co-propagating undulator radiation field induces an energy modulation of electrons that yields current modulation of the bunch due to the dispersion of the undulator dipole fields, known as microbunching. It means that the electrons are grouped into small bunches separated by a fixed distance that resonantly coincides with the wavelength of the radiation field. Consequently, the radiation field can be amplified coherently. In the absence of an initial resonant radiation field, a seed may build up from spontaneous incoherent emission in the SASE process.

The design of the FEL-based EUV light source is carried out using one-dimensional FEL theory as follows[32]. The FEL amplification takes place in an undulator with undulator period λ_u and peak magnetic field B_u at a resonant wavelength λ_X given by

$$\lambda_X = \frac{\lambda_u}{2\gamma^2}\left(1 + \frac{K^2}{2}\right), \qquad (21)$$

where $\gamma = E_b/m_e c^2$ is the relativistic factor of the electron beam energy E_b, and $K_u = 0.934 B_u \,(\text{T})\lambda_u \,(\text{cm}) = \gamma\theta_e$ is the undulator parameter, which is related to the maximum electron deflection angle θ_e. In the high-gain regime required for the operation of a SASE FEL, an important parameter is the Pierce parameter ρ_{FEL}, given by

$$\rho_{\text{FEL}} = \frac{1}{2\gamma}\left[\frac{I_b}{I_A}\left(\frac{\lambda_u K_u A_u}{2\pi\sigma_b}\right)^2\right]^{1/3}, \qquad (22)$$

where I_b is the beam current, $I_A = 17$ kA is the Alfven current, σ_b is the r.m.s transverse size of the electron bunch, and the coupling factor is $A_u = 1$ for a helical undulator and $A_u = J_0(\Xi) - J_1(\Xi)$ for a planar undulator, where $\Xi = K_u^2/[4(1 + K_u^2/2)]$ and J_0 and J_1 are Bessel functions of the first kind. Another important dimensionless parameter is the longitudinal velocity spread Λ of the beam normalized by the Pierce parameter:

$$\Lambda^2 = \frac{1}{\rho_{\text{FEL}}^2}\left[\left(\frac{\sigma_\gamma}{\gamma}\right)^2 + \left(\frac{\varepsilon\lambda_u}{4\lambda_X\beta}\right)^2\right]$$
$$= \frac{1}{\rho_{\text{FEL}}^2}\left[\left(\frac{\sigma_\gamma}{\gamma}\right)^2 + \left(\frac{\varepsilon_n^2}{2\sigma_b^2(1 + K_u^2/2)}\right)^2\right], \qquad (23)$$

where σ_γ/γ is the relativistic r.m.s. energy spread, ε is the r.m.s. transverse emittance, $\beta = \sigma_b^2/\varepsilon$ is the beta function provided by the guiding field (undulator plus external focusing) and ε_n is the normalized emittance, defined as $\varepsilon_n \equiv \gamma\varepsilon$, assuming that the beta function is constant along the length of the undulator. The e-folding gain length L_{gain} over which the power grows exponentially according to $\exp(2s/L_{\text{gain}})$ is given by

$$L_{\text{gain}} = \frac{\lambda_u}{4\pi\sqrt{3}\rho_{\text{FEL}}}(1 + \Lambda^2). \qquad (24)$$

In order to minimize the gain length, one needs a large Pierce parameter ρ_{FEL} and a normalized longitudinal velocity spread Λ sufficiently low compared to unity, which means a sufficiently small energy spread σ_γ/γ and ε. This expression applies to a moderately small beam size σ_b such that the diffraction parameter $B \gg 1$, where B is defined as

$$B = \frac{16\pi^2 A_u \sigma_b^2}{\lambda_X\lambda_u}\left[\frac{K_u^2/2}{\gamma(1 + K_u^2/2)}\frac{I_b}{I_A}\right]^{1/2}. \qquad (25)$$

The saturation length L_{sat} required to saturate the amplification can be expressed as

$$L_{\text{sat}} = L_{\text{gain}}\ln\left[\left(\frac{\Lambda^2 + 3/2}{\Lambda^2 + 1/6}\right)\frac{P_{\text{sat}}}{P_{\text{in}}}\right], \qquad (26)$$

where P_{in} and P_{sat} are the input power and the saturated power, which are related to the electron beam power P_b according to

$$P_b = \gamma I_b m_e c^2 = I_b E_b,$$
$$P_{\text{sat}} \cong 1.37\rho_{\text{FEL}}P_b\exp(-0.82\Lambda^2),$$
$$P_{\text{in}} \cong 3\sqrt{4\pi}\rho_{\text{FEL}}^2 P_b[N_{\lambda_X}\ln(N_{\lambda_X}/\rho_{\text{FEL}})]^{-1/2}, \qquad (27)$$

where N_{λ_X} is the number of electrons per wavelength, given by $N_{\lambda_X} = I_b\lambda_X/(ec)$.

For an EUV light source based on a FEL, a planar undulator comprising alternating dipole magnets is used, e.g., a pure permanent magnet (PPM) undulator with $Nd_2Fe_{14}B$ (Nd–Fe–B) blocks or a hybrid undulator comprising PPMs and ferromagnetic poles, e.g., a high saturation cobalt steel such as Vanadium Permendur or a simple iron. For a hybrid undulator, the thickness of the pole and magnet is optimized in order to maximize the peak field. The peak field B_u of the gap is estimated in terms of the gap g and period λ_u according to $B_u = a\,(\text{T})\exp[b(g/\lambda_u) + c(g/\lambda_u)^2]$ for a gap range $0.1 < g/\lambda_u < 1$, where $a = 3.694$ T, $b = -5.068$ and $c = 1.520$ for the hybrid undulator with Vanadium Permendur. Table 1 summarizes design examples for a fiber laser-driven laser plasma accelerator-based FEL-produced EUV radiation source at 13.5 nm wavelength using undulators with periods 5 mm (Case A), 10 mm (Case B), 15 mm (Case C), 20 mm (Case D), and 25 mm (Case E), all cases of which have the same gap:period ratio 0.2, e.g., $g = 1$ mm (Case A), 2 mm (Case B), 3 mm (Case C), 4 mm (Case D), and 5 mm (Case E), respectively. The bunch duration of the electron beam in the injector stage at a plasma density of $n_e \approx 10^{18}$ cm^{-3} is assumed to be ~ 10 fs full-width at half-maximum (FWHM), based on a

Table 1. Parameters for laser plasma accelerator-based EUV FEL light sources.

Case	A	B	C	D	E
Laser					
Laser wavelength (μm)	1	1	1	1	1
Average laser power (MW)	1.63	1.24	1.19	1.22	1.27
Repetition rate (MHz)	1.22	0.515	0.315	0.223	0.168
Laser energy per pulse (J)	1.34	2.40	3.79	5.52	7.57
Peak power (TW)	29	43	59	75	93
Pulse duration (fs)	46	56	65	73	82
Matched spot radius (μm)	19	23	27	30	34
Laser plasma accelerator					
Electron beam energy (MeV)	243	427	659	937	1257
Plasma density (10^{17} cm^{-3})	8.3	5.6	4.2	3.2	2.6
Accelerator length (mm)	18	32	51	74	102
Charge per bunch (nC)	0.5	0.5	0.5	0.5	0.5
Field reduction factor α	0.223	0.267	0.302	0.325	0.364
Bunch duration (fs)	10	10	10	10	10
Energy spread (%)	∼1.1	∼1.5	∼1.6	∼1.6	∼1.6
Transverse beam size (μm)	25	25	25	25	25
Peak current (kA)	50	50	50	50	50
Average beam power (kW)	148	110	104	104	105
Efficiency of laser to beam (%)	9.1	8.9	8.7	8.5	8.3
Free electron laser					
Undulator period (mm)	5	10	15	20	25
Radiation wavelength (nm)	13.5	13.5	13.5	13.5	13.5
Gap (mm)	1	2	3	4	5
Peak magnetic field (T)	1.425	1.425	1.425	1.425	1.425
Undulator parameter K_u	0.666	1.33	2.00	2.66	3.33
Pierce parameter (%)	1.12	1.51	1.60	1.60	1.57
Gain length (mm)	41	61	86	115	146
Saturation length (mm)	499	721	1016	1355	1723
Number of periods	100	72	68	68	69
Spectral bandwidth (%)	1.0	1.4	1.5	1.5	1.5
R.m.s. radiation cone angle (μrad)	116	97	82	71	63
Input power (MW)	0.94	3.03	5.26	7.48	9.72
Saturated power (GW)	82	194	317	451	596
Duration of EUV pulse (fs)	10	10	10	10	10
Average EUV power (kW)	1	1	1	1	1
Efficiency of EUV generation (%)	0.061	0.081	0.084	0.082	0.079

measurement of the electron bunch duration in a recent laser wakefield acceleration experiment[33]. The relative energy spread of the accelerated electron beam with an injection energy of $0.1E_b$, where E_b is the final beam energy in the accelerator stage, is assumed to be of the order of 10% in the injector stage. After acceleration up to 10 times higher energy in the accelerator stage, the relative energy spread at the final beam energy is reduced to $\Delta E/E_b \sim 1\%$ due to adiabatic damping in the longitudinal beam dynamics. The transverse beam size is tuned by employing a beam focusing system. Figure 1 shows a schematic of the EUV light source based on a compact FEL driven by a fiber laser-based plasma accelerator.

2.5. Design of all-optical Gamma-beam source

The design of a Gamma-beam source based on inverse Compton scattering is carried out by using a result of quantum electrodynamics on photon–electron interactions, namely, the Klein–Nishina formula, which gives the differential cross section of photons scattered from a single electron in the lowest order of quantum electrodynamics. In Compton scattering of a laser photon with energy $\hbar\omega_L$ ($\hbar\omega_L$ (eV) $= 1.240/\lambda_L$ (μm) for laser wavelength λ_L (μm)) off a beam electron, the maximum energy of the scattered photon is given by $E_{\gamma\,\text{max}} = 4\gamma_e^2 a\hbar\omega_L$, where $\gamma_e = E_b/m_e c^2$ is the relativistic factor for an electron beam energy E_b with electron rest mass $m_e c^2 \simeq 0.511$ MeV and the factor $a = [1 + 4\gamma_e(\hbar\omega_L/m_e c^2)]^{-1}$. In the laboratory frame, the differential cross section of Compton scattering[34] is given by

$$\frac{d\sigma}{d\kappa} = 2\pi a r_e^2 \left\{ 1 + \frac{\kappa^2(1-a)^2}{1-\kappa(1-a)} + \left[\frac{1-\kappa(1+a)}{1-\kappa(1-a)} \right]^2 \right\}, \tag{28}$$

where $\kappa = E_\gamma/E_{\gamma\,\text{max}}$ is the energy of a scattered photon normalized by the maximum photon energy and $r_e^2 \simeq 79.4$ mb (1 barn $= 10^{-24}$ cm^2) with the classical electron radius r_e. In the laboratory frame, the scattering angle θ of the photon is given by $\tan\theta = \gamma_e^{-1}\sqrt{(1-\kappa)/a\kappa}$. Integrating the differential cross section over $0 \leqslant \kappa \leqslant 1$, the total cross section of Compton scattering becomes

$$\sigma_{\text{total}} = \pi r_e^2 a \left[\frac{2a^2 + 12a + 2}{(1-a)^2} + a - 1 \right.$$
$$\left. + \frac{6a^2 + 12a - 2}{(1-a)^3} \ln a \right]. \tag{29}$$

This total cross section leads to a cross section of Thomson scattering $\sigma_{\text{Thomson}} = 8\pi r_e^2/3 = 665$ mb for an electron beam energy $E_b \to 0$. The fractional cross section for the photon energy range $E_{\gamma\,\text{max}} - \Delta E_\gamma \leqslant E_\gamma \leqslant E_{\gamma\,\text{max}}$ is given by

$$\Delta\sigma = 2\pi a r_e^2 \Delta\kappa \left[\left(\frac{1+a}{1-a} \right)^2 + \frac{4}{(1-a)^2} \right.$$
$$\times \left(1 + \frac{1-a}{a}\Delta\kappa \right)^{-1} + (a-1)\left(1 + \frac{\Delta\kappa}{2} \right)$$
$$\left. + \frac{1-6a-3a^2}{(1-a)^3\Delta\kappa} \ln\left(1 + \frac{1-a}{a}\Delta\kappa \right) \right], \tag{30}$$

with $\Delta\kappa = \Delta E_\gamma/E_{\gamma\,\text{max}} \ll 1$. All photons in this energy range are scattered in the forward direction within a half-cone angle $\theta \sim \gamma_e^{-1}\sqrt{\Delta\kappa/a}$. For an electron beam interacting with a laser pulse at an angle of α_{int} in the horizontal
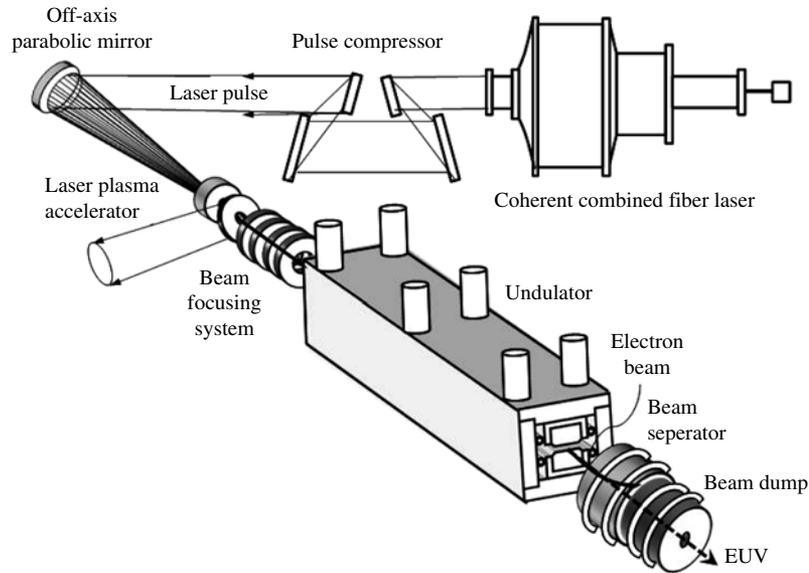
Figure 1. Schematic of the EUV light source based on a compact FEL driven by a fiber laser-based plasma accelerator.

plane (x-plane), the luminosity representing the probability of collisions between electron and laser beams per unit cross section per unit time is obtained by L (mb^{-1}s^{-1}) = $N_e N_L f_L / 2\pi \Sigma$, where N_e is the number of electrons contained in the electron bunch, N_L is the number of photons per laser pulse, f_L is the repetition rate of laser pulses, and Σ is the area where the two beams overlap, given by

$$\Sigma = (\sigma_{ey}^2 + \sigma_{Ly}^2)^{1/2}[\cos^2(\alpha_{int}/2)(\sigma_{ex}^2 + \sigma_{Lx}^2) + \sin^2(\alpha_{int}/2)(\sigma_{ez}^2 + \sigma_{Lz}^2)]^{1/2}, \quad (31)$$

where σ_{ex} and σ_{ey} are the r.m.s. horizontal and vertical sizes of the electron beam, σ_{ez} is the r.m.s. bunch length of the electron beam, σ_{Lx} and σ_{Ly} are the r.m.s. horizontal and vertical spot sizes of the laser beam, and σ_{Lz} is the r.m.s. pulse length of the laser beam. For a head-on collision providing efficient Gamma-beam production, the crossing angle between the electron and laser beams is chosen to be $\alpha_{int} = 0$. Tuning the beam focusing system and the interaction optics so as to give $\sigma_{ex} \approx \sigma_{ey} \approx \sigma_{Lx} \approx \sigma_{Ly}$, the luminosity turns out to be $L = N_e N_L f_L / (4\pi r_{int}^2)$, where r_{int} is the laser spot radius at the interaction point. Using $N_e = 1.6022 \times 10^{10}(Q_e/1 \text{ nC})$ and $N_L = U_{LS}/\hbar\omega_L = 5.0334 \times 10^{18}U_{LS}$ (J)λ_L(μm), where Q_e is the charge of the electron bunch and $U_{LS} = P_{LS}\tau_{LS}$ is the energy of a scatter pulse with peak power P_{LS} and duration τ_{LS}, the luminosity is calculated as

$$L \text{ (mb}^{-1}\text{s}^{-1}) = Q_e I_{int} f_L \tau_{LS}/(8e\hbar\omega_L)$$
$$\approx 1.0 \times 10^{-14} f_L \text{ (s}^{-1})Q_e \text{ (nC)}$$
$$\times I_{int}(\text{W cm}^{-2})\tau_{LS}(\text{fs})\lambda_L \text{ (μm)}, \quad (32)$$

where I_{int} is the focused intensity of the scatter pulse at the interaction point. Thus the Gamma-beam flux is given by

$$N_\gamma \text{ (s}^{-1}) = L\sigma_{tot} \approx 1 \times 10^{-14}\sigma_{tot} \text{ (mb) } f_L \text{ (s}^{-1})Q_e \text{ (nC)}$$
$$\times I_{int} \text{ (W cm}^{-2})\tau \text{ (fs)}\lambda_L(\text{μm}). \quad (33)$$

The fractional Gamma-beam flux with photon energy spread $\Delta\kappa = \Delta E_\gamma / E_{\gamma \text{ max}}$ is estimated as

$$\Delta N_\gamma \text{ (s}^{-1}) = L\Delta\sigma \approx 1 \times 10^{-14}\Delta\sigma \text{ (mb) } f_L \text{ (s}^{-1})Q_e \text{ (nC)}$$
$$\times I_L(\text{W cm}^{-2})\tau(\text{fs})\lambda_L \text{ (μm}). \quad (34)$$

Table 2 summarizes design examples for an all-optical laser plasma accelerator-based Gamma-beam source at photon energies 2.5 MeV (Case A), 5 MeV (Case B), 10 MeV (Case C), 15 MeV (Case D), and 20 MeV (Case E), respectively. Figure 2 is a schematic illustration of the Gamma-beam source based on inverse Compton scattering off relativistic electron beams driven by a laser plasma accelerator.

3. Conclusion

We present methods for producing EUV light at a wavelength of 13.5 nm from a SASE FEL generated by electron beams from a laser plasma accelerator driven by a fiber-based CPA laser and also for producing a Gamma beam with photon energies of 1–20 MeV via inverse Compton scattering off relativistic electron beams from a laser plasma accelerator. For these practical applications of laser plasma accelerators, it is essential to employ high average power,
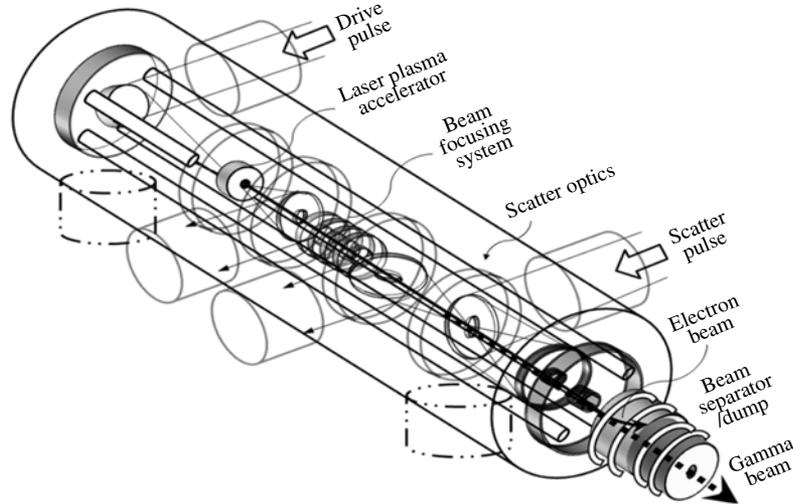
Figure 2. Schematic illustration of the Gamma-beam source based on inverse Compton scattering off relativistic electron beams driven by a laser plasma accelerator.

Table 2. Parameters for all-optical laser plasma accelerator-based Gamma-beam sources.

Case	A	B	C	D	E
Laser plasma accelerator					
Laser wavelength (μm)	0.8	0.8	0.8	0.8	0.8
Repetition rate (Hz)	10	10	10	10	10
Laser energy per pulse (J)	1.78	2.56	3.68	4.55	5.31
Peak power (TW)	41	52	66	77	85
Pulse duration (fs)	43	49	55	59	62
Matched spot radius (μm)	18	20	23	24	26
Electron beam energy (MeV)	326	461	654	802	928
Plasma density (10^{17} cm^{-3})	9.2	7.3	5.7	4.9	4.5
Accelerator length (mm)	24	34	50	61	72
Charge per bunch (nC)	0.5	0.5	0.5	0.5	0.5
Bunch duration (fs)	~10	~10	~10	~10	~10
Transverse beam size (μm)	25	25	25	25	25
Compton scatter					
Photon energy (MeV)	2.5	5	10	15	20
Laser peak power (TW)	10	10	10	10	10
Pulse duration (fs)	250	250	250	250	250
Pulse energy (J)	2.5	2.5	2.5	2.5	2.5
Laser spot radius (μm)	25	25	25	25	25
Focused intensity (10^{18} W cm^{-2})	1	1	1	1	1
Repetition rate (Hz)	10	10	10	10	10
Luminosity (10^6 mb^{-1} s^{-1})	10	10	10	10	10
Total cross section (mb)	660	658	655	653	651
Total photon flux (10^9 s^{-1})	6.60	6.58	6.55	6.53	6.51
Spectral bandwidth (%)	1.0	1.0	1.0	1.0	1.0
Scattering angle within 1% BW (μrad)	313	222	157	128	111
Cross section within 1% BW (mb)	9.80	9.77	9.73	9.69	9.66
Photon flux within 1% BW (10^8 s^{-1})	0.980	0.977	0.973	0.969	0.966

source can produce a high-quality photon flux of 3×10^{12} s^{-1} at 10 MeV energy within a 1% bandwidth. One such high average power laser is a coherent combining fiber laser system[35], comprising a plurality of amplifying fibers wherein an initial laser pulse is distributed and amplified to a 1 mJ level, intended for grouping together the elementary pulses amplified in the fiber in order to form a single amplified global laser pulse with a 1 J level energy.

In both radiation sources, beam transport and imaging from the laser plasma accelerator to the undulator or a focal point of the scatter laser pulse is provided by a beam focusing system that comprises Halbach-type permanent quadrupole magnets made of NdFeB-type rare-earth magnets with a high remanent field[36, 37]. According to simulation results on ionization-induced injection at a plasma density $n_e \approx 10^{18}$ cm^{-3}[31], the normalized emittance is assumed to be $\varepsilon_n \approx 1$ μm inside the wakefield. The transverse beam size in the beam transport optics is given by $\sigma_b = \sqrt{\beta \varepsilon_n / \gamma}$, where β is the beta function of the beam optics at the undulator or the scattering point. For Case C in Table 1, the beta function should be set to $\beta = \gamma \sigma_b^2 / \varepsilon_n \approx 80$ cm inside the undulator. The electron beam, after passing through the undulator or being scattered by the scatter laser pulse, is bent by the dipole field of a permanent magnet (a beam separator) made of NdFeB material and dumped to a copper beam dump with a water cooling element, while the EUV radiation or the Gamma beam is extracted from a beam separator and directed to an EUV lithography scanner or a photon beam irradiation system.

Acknowledgements

high efficiency drive lasers operating at high repetition pulse rates (of the order of 300 kHz); the corresponding average power of 1 MW means that the EUV FEL is capable of producing an average radiation power of 1 kW at a wavelength of 13.5 nm and the all-optical Gamma beam

Shanghai Jiao Tong University, Institute of Physics, CAS, China, and the Center for Relativistic Laser Science, Institute for Basic Science (IBS), Korea.

References

1. T. Tajima and J. M. Dawson, Phys. Rev. Lett. **43**, 267 (1979).
2. W. P. Leemans, B. Nagler, A. J. Gonsalves, C. Toth, K. Nakamura, C. G. R. Geddes, E. Esarey, C. B. Schroeder, and S. M. Hooker, Nat. Phys. **2**, 696 (2006).
3. C. E. Clayton, J. E. Ralph, F. Albert, R. A. Fonseca, S. H. Glenzer, C. Joshi, W. Lu, K. A. Marsh, S. F. Martins, W. B. Mori, A. Pak, F. S. Tsung, B. B. Pollock, J. S. Ross, L. O. Silva, and D. H. Froula, Phys. Rev. Lett. **105**, 105003 (2010).
4. H. Lu, M. Liu, W. Wang, C. Wang, J. Liu, A. Deng, J. Xu, C. Xia, W. Li, H. Zhang, X. Lu, C. Wang, J. Wang, X. Liang, Y. Leng, B. Shen, K. Nakajima, R. Li, and Z. Xu, Appl. Phys. Lett. **99**, 091502 (2011).
5. X. Wang, R. Zgadzaj, N. Fazel, Z. Li, S. A. Yi, X. Zhang, W. Henderson, Y. Y. Chang, R. Korzekwa, H. E. Tsai, C. H. Pai, H. Quevedo, G. Dyer, E. Gaul, M. Martinez, A. C. Bernstein, T. Borger, M. Spinks, M. Donovan, V. Khudik, G. Shvets, T. Ditmire, and M. C. Downer, Nat. Commun. **4**, 1988 (2013).
6. H. T. Kim, K. H. Pae, H. J. Cha, I. J. Kim, T. J. Yu, J. H. Sung, S. K. Lee, T. M. Jeong, and J. Lee, Phys. Rev. Lett. **111**, 165002 (2013).
7. T. Kameshima, W. Hong, K. Sugiyama, X. Wen, Y. Wu, C. Tang, Q. Zhu, Y. Gu, B. Zhang, H. Peng, S.-I. Kurokawa, L. Chen, T. Tajima, T. Kumita, and K. Nakajima, Appl. Phys. Exp. **1**, 066001 (2008).
8. S. Karsch, J. Osterhoff, A. Popp, T. P. Rowlands-Rees, Z. Major, M. Fuchs, B. Marx, R. Hörlein, K. Schmid, L. Veisz, S. Becker, U. Schramm, B. Hidding, G. Pretzler, D. Habs, F. Grüner, F. Krausz, and S. M. Hooker, New J. Phys. **9**, 415 (2007).
9. O. Lundh, J. Lim, C. Rechatin, L. Ammoura, A. Ben-Ismail, X. Davoine, G. Gallot, J. P. Goddet, E. Lefebvre, V. Malka, and J. Faure, Nat. Phys. **7**, 219 (2011).
10. N. A. M. Hafz, T. M. Jeong, I. W. Choi, S. K. Lee, K. H. Pae, V. V. Kulagin, J. H. Sung, T. J. Yu, K.-H. Hong, T. Hosokai, J. R. Cary, D.-K. Ko, and J. Lee, Nat. Photon. **2**, 571 (2008).
11. J. S. Liu, C. Q. Xia, W. T. Wang, H. Y. Lu, C. Wang, A. H. Deng, W. T. Li, H. Zhang, X. Y. Liang, Y. X. Leng, X. M. Lu, C. Wang, J. Z. Wang, K. Nakajima, R. X. Li, and Z. Z. Xu, Phys. Rev. Lett. **107**, 035001 (2011).
12. B. B. Pollock, C. E. Clayton, J. E. Ralph, F. Albert, A. Davidson, L. Divol, C. Filip, S. H. Glenzer, K. Herpoldt, W. Lu, K. A. Marsh, J. Meinecke, W. B. Mori, A. Pak, T. C. Rensink, J. S. Ross, J. Shaw, G. R. Tynan, C. Joshi, and D. H. Froula, Phys. Rev. Lett. **107**, 045001 (2011).
13. W. T. Wang, W. T. Li, J. S. Liu, C. Wang, Q. Chen, Z. J. Zhang, R. Qi, Y. X. Leng, X. Y. Liang, Y. Q. Liu, X. M. Lu, C. Wang, R. X. Li, and Z. Z. Xu, Appl. Phys. Lett. **103**, 243501 (2013).
14. A. Pak, K. A. Marsh, S. F. Martins, W. Lu, W. B. Mori, and C. Joshi, Phys. Rev. Lett. **104**, 025003 (2010).
15. C. McGuffey, A. G. R. Thomas, W. Schumaker, T. Matsuoka, V. Chvykov, F. J. Dollar, G. Kalintchenko, V. Yanovsky, A. Maksimchuk, K. Krushelnick, V. Y. Bychenkov, I. V. Glazyrin, and A. V. Karpeev, Phys. Rev. Lett. **104**, 025004 (2010).
16. C. Xia, J. Liu, W. Wang, H. Lu, W. Cheng, A. Deng, W. Li, H. Zhang, X. Liang, Y. Leng, X. Lu, C. Wang, J. Wang, K. Nakajima, R. Li, and Z. Xu, Phys. Plasmas **18**, 113101 (2011).
17. W. T. Li, J. S. Liu, W. T. Wang, Z. J. Zhang, Q. Chen, Y. Tian, R. Qi, C. H. Yu, C. Wang, T. Tajima, R. X. Li, and Z. Z. Xu, Appl. Phys. Lett. **104**, 093510 (2014).
18. W. Leemans, C. G. R. Geddes, J. Faure, Cs. Tóth, J. van Tilborg, C. B. Schroeder, E. Esarey, and G. Fubiani, Phys. Rev. Lett. **91**, 074802 (2003).
19. Z. D. Hu, Z. M. Sheng, W. M. Wang, L. M. Chen, Y. T. Li, and J. Zhang, Phys. Plasmas **20**, 080702 (2013).
20. M. Fuchs, R. Weingartner, A. Popp, Zs. Major, S. Becker, J. Osterhoff, I. Cortrie, B. Benno Zeitler, R. Rainer Hörlein, G. D. Tsakiris, U. Schramm, T. P. Rowlands-Rees, S. M. Hooker, D. Habs, F. Krausz, S. Karsch, and F. Grüner, Nat. Phys. **5**, 826 (2009).
21. S. Kneip, C. McGuffey, J. L. Martins, S. F. Martins, C. Bellei, V. Chvykov, F. Dollar, R. Fonseca, C. Huntington, G. Kalintchenko, A. Maksimchuk, S. P. D. Mangles, T. Matsuoka, S. R. Nagel, C. A. J. Palmer, J. Schreiber, K. Ta Phuoc, A. G. R. Thomas, V. Yanovsky, L. O. Silva, K. Krushelnick, and Z. Najmudin, Nat. Phys. **6**, 980 (2010).
22. W. T. Yan, L. M. Chen, D. Z. Li, L. Zhang, N. A. M. Hafz, J. Dunn, Y. Ma, K. Hung, L. Su, M. Chen, Z. M. Sheng, and J. Zhang, Proc. Natl. Acad. Sci. **111**, 5825 (2014).
23. S. Cipiccia, M. R. Islam, B. Ersfeld, R. P. Shanks, E. Brunetti, G. Vieux, X. Yang, R. C. Issac, S. M. Wiggins, G. H. Welsh, M.-P. Anania, D. Maneuski, R. Montgomery, G. Smith, M. Hoek, D. J. Hamilton, N. R. C. Lemos, D. Symes, P. P. Rajeev, V. O. Shea, J. M. Dias, and D. A. Jaroszynski, Nat. Phys. **7**, 867 (2011).
24. K. Ta Phuoc, S. Corde, C. Thaury, V. Malka, A. Tafzi, J. P. Goddet, R. C. Shah, S. Sebban, and A. Rousse, Nat. Photon. **6**, 308 (2012).
25. N. D. Powers, I. Ghebregziabher, G. Golovin, C. Liu, S. Chen, S. Banerjee, J. Zhang, and D. P. Umstadter, Nat. Photon. **8**, 28 (2014).
26. I. Kostyukov, A. Pukhov, and S. Kiselev, Phys. Plasmas **11**, 5256 (2004).
27. W. Lu, M. Tzoufras, C. Joshi, F. S. Tsung, W. B. Mori, J. Vieira, R. A. Fonseca, and L. O. Silva, Phys. Rev. ST Accel. Beams **10**, 061301 (2007).
28. K. Nakajima, H. Lu, X. Zhao, B. Shen, R. Li, and Z. Xu, Chin. Opt. Lett. **11**, 013501 (2013).
29. K. Nakajima, A. Deng, X. Zhang, B. Shen, J. Liu, R. Li, Z. Xu, T. Ostermayr, S. Petrovics, C. Klier, K. Iqbal, H. Ruhl, and T. Tajima, Phys. Rev. ST Accel. Beams **14**, 091301 (2011).
30. S. Kalmykov, A. Yi, V. Khudik, and G. Shvets, Phys. Rev. Lett. **103**, 135004 (2009).
31. M. Chen, E. Esarey, C. B. Schroeder, C. G. R. Geddes, and W. P. Leemans, Phys. Plasmas **19**, 033101 (2012).
32. P. Elleaume, J. Chavanne, and B. Faatz, Nucl. Instrum. Methods Phys. Res. A **455**, 503 (2000).
33. A. Buck, M. Nicolai, K. Schmid, C. M. S. Sears, A. Sävert, J. M. Mikhailova, F. Krausz, M. C. Kaluza, and L. Veisz, Nat. Phys. **7**, 543 (2011).
34. H. A. Tolhokk, Rev. Mod. Phys. **28**, 277 (1956).
35. G. Mourou, B. Brocklesby, T. Tajima, and J. Limpert, Nat. Photon. **7**, 258 (2013).
36. J. K. Lim, P. Frigola, G. Travish, J. B. Rosenzweig, S. G. Anderson, W. J. Brown, J. S. Jacob, C. L. Robbins, and A. M. Tremaine, Phys. Rev. ST Accel. Beams **8**, 0072401 (2005).
37. K. Nakajima, A. H. Deng, H. Yoshitama, N. A. M. Hafz, H. Y. Lu, B. F. Shen, J. S. Liu, R. X. Li, and Z. Z. Xu, *Free Electron Laser* Chap. 5, S. Varró, ed. p. 119 (InTech, Rijeka, Croatia, 2012).